In situ structural studies of the underpotential deposition of copper onto an iodine covered platinum surface using x-ray standing waves

G. M. Bommarito, D. Acevedo, J. R. Rodriguez and H. D. Abruña*

Department of Chemistry, Baker Laboratory, Cornell University
Ithaca, New York, 14853

ABSTRACT

We present initial results of an *in situ* structural investigation of the underpotential deposition of copper on an iodine covered platinum/carbon layered synthetic microstructure, using x-ray standing waves generated by specular (total external) reflection and Bragg diffraction. We also compare the result of surface coverage isotherms derived from both electrochemical and x-ray measurements.

1. INTRODUCTION

The underpotential deposition (UPD) process has been extensively studied during the past two decades due to its theoretical and practical importance in fields such as: electrocrystallization, catalysis, and surface chemistry. In this process, submonolayer to monolayer(s) amounts of a metal can be electrodeposited on a foreign metal substrate in a quantifiable and reproducible fashion prior to bulk deposition. Numerous electrochemical and spectroscopic techniques have been utilized to probe the mechanism(s) of formation, and the structural properties of UPD layers.

Conventional electrochemical methods have been used to obtain thermodynamic and kinetic information about the UPD process[1-2]. Cyclic voltammetry[1] and current transient[2] experiments are the methods of choice in these types of studies. Structural features of the UPD layer were first derived, indirectly, from equilibrium-coverage potential isotherms using single crystal substrates[3]. Non-monotonic current transients have been observed in a number of experiments[2], and these have been explained in terms of mechanisms involving nucleation and growth processes. Although electrochemical methods are invaluable in controlling and measuring thermodynamic parameters such as applied potential, charge, and coverage, any structural inferences are always indirect and often model dependent.

Direct atomic structural reports were presented by Kolb *et al.*, on the UPD of copper on gold single crystals using reflected high energy electron diffraction (RHEED)[4]. Because of the experiment's nature, the electrode was emersed from solution, introducing some uncertainty regarding the structural integrity of the double layer, since potential control was lost upon removal of the electrode from solution. Hubbard *et al.* also used electron spectroscopic techniques to obtain direct atomic structural information about metal deposits on an iodine covered Pt(111) surface[5]. They found that electrodeposition occurred in a well-defined manner, with the formation of different film structures depending on the coverage. Although these *ex situ* experiments provided a wealth of information, it is unclear what structural changes to the UPD layer the electrode transfer from solution to vacuum may have caused. In addition, these experiments do not provide structural information about the solution side of the double layer, an integral part of the system at equilibrium with the adsorbed species.

In recent years, the use of atomic resolution microscopic techniques has provided the means to obtain *in situ* direct atomic structural information from UPD system. Scanning tunneling and atomic force microscopy have been recently used to study the electrodeposition of copper on gold surfaces[6]. These studies have shown that the UPD process occurrs in a well-defined manner and the structures observed from these experiments are similar to those observed in vacuum. As that was the case in the *ex situ* experiments, these techniques provide information only for the deposited layer.

Recently, *in situ* x-ray spectroscopic and diffraction techniques have provided unique atomic resolution structural information about UPD systems. Extended x-ray absorption fine structure (EXAFS) and x-ray absorption near edge structure (XANES) have been widely used to study various UPD systems[7], providing information about the local structure atomic environment and the oxidation state of the adsorbed species. Furthermore, surface x-ray scattering measurements have been used to study the in-plane structure of the UPD layer for specific cases[8]. In addition to these techniques, x-ray standing waves (XSW) have been utilized to probe the electrochemical double layer[9]. In these studies, one can obtain information pertaining to the distribution of species, including the diffuse layer, in a direction normal to the substrate's surface.

In this paper, we present the results of a series of *in situ* x-ray standing wave experiments aimed at probing the potential dependent structural nature of the underpotential deposition of copper on an iodine covered platinum/carbon layered synthetic microstructure.

2. THEORETICAL BACKGROUND

X-ray standing waves are generated when coherently related incident and reflected plane waves interfere (Figure 2.1). The standing wave electric field intensity is given by

$$I(\theta,z)=|\varepsilon_O+\varepsilon_R|^2=|E_O|^2\left[1+R+2\sqrt{R}\cos(\upsilon-2\pi Qz)\right] \tag{1}$$

where

$$\varepsilon_{O,R}=E_{O,R}\exp\left\{i\left[\omega t-2(k_x x-k_z z)\right]\right\} \tag{2}$$

are the incident and reflected plane waves if their respective wavevectors k_O and k_R lie in the x-z plane with the z axis normal to the substrate's surface. $Q=k_O-k_R$ is the momentum transfer with a magnitude given by

$$|Q|=Q=\frac{2\sin\theta}{\lambda} \tag{3}$$

At the Bragg angle (θ_B), $Q=1/d$ where d is the substrate's characteristic d-spacing. The angular dependence of Equation (1) is contained within the variables $R(\theta)$ and $\upsilon(\theta)$ which correspond, respectively, to the intensity and the phase of the reflected wave relative to the incident one. During specular reflection (total external reflection) and Bragg diffraction a strong, well-defined standing wave field is generated. In addition as the angle of incidence θ is scanned across these reflection regimes, there is a change of π in the relative phase $\upsilon(\theta)$, causing the nodal and antinodal planes of the standing wave field to move inward in a direction normal to the substrate's surface (we confine our discussion here to the case where the diffraction planes of the substrate are parallel to the surface). Since the relative phase and the standing wave periodicity are known exactly at all angles θ in both the specular reflection and Bragg diffraction regimes, the position of the nodal and antinodal planes in the standing wave with respect to the substrate's surface is also known exactly as a function of θ. Since the

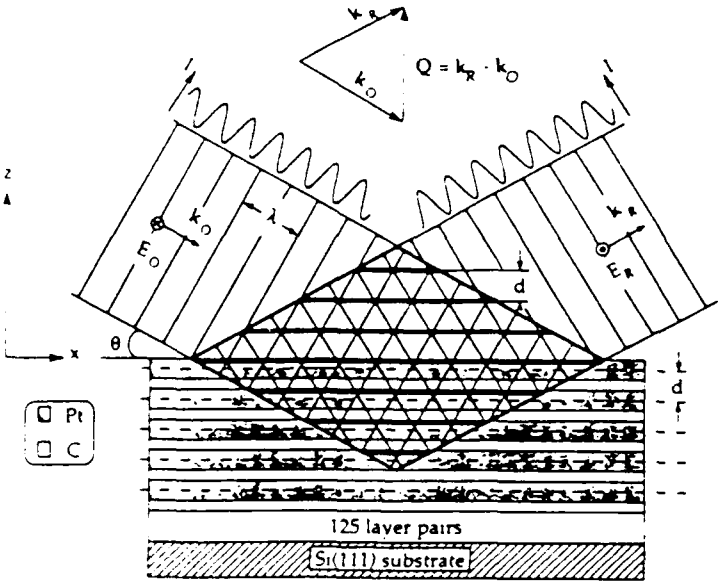

Figure 2.1 Illustration of the x-ray standing wave generated by the interference of the coherently related incident and Bragg diffracted plane waves for a platinum/carbon LSM. The solid lines indicate the antinodes of the incident and diffracted waves, the bold lines point out the antinodes of the standing wave, and the dashed lines mark the position of the diffraction planes in the LSM.

photoelectric effect for core electrons is directly proportional, in the dipole approximation, to the electric field intensity at the center of an atom, the emission yield (i.e. the fluorescence yield) from the atoms in an overlayer or a distribution of species above the substrate's surface will be uniquely modulated as a function of θ. To calculate this yield, the standing wave electric field intensity $I(\theta,z)$ must be integreated over the entire distribution N(z):

$$Y(\theta) = \int_0^{\infty} I(\theta,z)N(z)dz \tag{4}$$

Conventionally, XSWs are generated by dynamical Bragg diffraction from perfect single crystals[10]. In this work, we are interested in studying structural changes not only for an atomic overlayer but also for extended distributions of species (on the order of tens to hundreds of A). The periodicity of standing waves generated from a perfect single crystal is too short to effectively measure these distributions. Thus, an alternative substrate must be used to create long period XSWs. In addition, electrochemical experiments require the substrate's surface to be metallic, since it also serves as the working electrode. Both constraints are fulfilled by using layered synthetic microstructures (LSMs) as mirror/diffracting structures. LSMs are artificial, depth-periodic structures, prepared by depositing alternating layers of high and low electron density elements, thus creating a superlattice structure with diffraction planes centered in the high electron density layers (Figure 2.1). The XSW technique using LSMs has been applied in several studies[9], and we refer the reader to these references for further details.

3. EXPERIMENTAL ASPECTS

The experiments were carried out at the Cornell High Energy Synchrotron Source (CHESS), under parasitic conditions (5GeV, 60-100 mA), using the B2 beam line. The experimental arrangement is shown in Figure 3.1. White beam radiation enters the

experimental hutch through a thin beryllium window and passes through a double-crystal Si(111) monochromator. The monochromator resolution was approximately 0.5 eV at 9.0 keV.

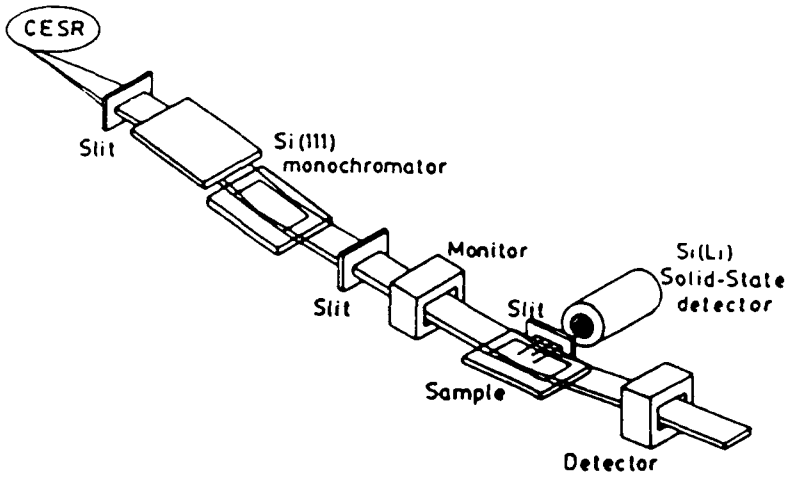

Figure 3.1 Experimental arrangement used in XSW measurements.

The emerging beam is collimated by vertical and horizontal slits. The beam incident onto the sample had a height and width of 0.04 and 4 mm, respectively. A high degree of collimation is needed because of the geometrical constraints imposed by the grazing incidence arrangement, and to ensure that, to a good approximation, the incident beam is a plane wave. The ion chambers measure the absolute reflectivity, while a Si(Li) solid-state detector is used in conjunction with a spectroscopic amplifier and a histogramming memory module to measure the fluorescence yield. The detector resolution was 150 eV at 6.0 keV. An x-ray energy of 9.35 keV was selected to excite copper K_α fluorescence. The incident flux was approximately 10^9 photons/s.

The electrochemical cell housed inside an aluminum holder, consisted of a cylindrical Teflon body with feedthroughs for electrolytes and electrode connections. The cell was thoroughly cleaned prior to use. The filling and rinsing of the cell with electrolyte was accomplished with pressurized glass vessels through the fluid feedthroughs. A thin layer of solution (approx.. 1-3 μm thick) was trapped between the electrode, and a 6.35μm thick polypropylene film which was held in place by a Teflon ring. All the electrochemical measurements were conducted with the polypropylene film distended by the addition of excess bulk electrolyte into the cell. The thin layer was then restored by removing excess electrolyte. Potential control of the electrode was retained through filling and rinsing stages. All applied potentials are reported with respect to a Ag/AgCl reference electrode.

Platinum/carbon LSMs of dimensions 15 mm by 20 mm were obtained from Ovonic Synthetic Materials Co. (Troy, MI). The LSMs used had d-spacings of 39.7 Å or 41.4 Å, and consisted of 200 layer pairs of platinum and carbon with platinum as the outermost layer deposited on a 0.015 in. thick Si(111) substrate.

For each XSW scan, the energy-dispersed fluorescence spectrum at a given angular position was recorded into 256 channels of the histogramming memory module. A typical scan consisted of 64 points over angular ranges of 10 mrad and 3.75 mrad for the specular reflection

and Bragg diffraction regions respectively, and took approximately 20 min. to complete. Approximately 2 min/point of data were collected for each potential studied.

Solutions were prepared with ultrapure reagents (Aldrich) and pyrolytically distilled water (PDW). Prior to use, solutions were degassed for over 30 min. with high purity nitrogen

4. ELECTROCHEMISTRY

UPD refers to the electrodeposition of metal monolayer(s) on a foreign metal substrate at potentials that can be significantly less negative than that for deposition on the same metal surface as the adsorbate. This phenomena allows for precise and reproducible control of the surface coverage, lending itself to studies of coverage dependent structure and electronic properties of a metallic ad-layer. Thus, *in situ* structural studies of UPD systems could elucidate aspects regarding lattice formation in terms of specific processes such as adsorption, charge transfer, surface diffusion, nucleation and growth, solution mass transport and double layer distributional changes. In addition, and of particular interest in this work, is the extent to which surface defects play a role in the dynamics of growth.

In these x-ray experiments, a platinum/carbon LSM is used as the diffracting substrate and working electrode. Some of the structural properties of this surface can be obtained directly form reflectivity measurements, as we will discuss later. Although indirectly, electrochemical measurements can also yield structural information regarding the LSM's platinum surface, by comparison to electrochemical experiments with electrode surfaces that are structurally well-defined. As an example, we show in Figure 4.1 the cyclic voltammetry in sulfate supporting electrolyte of different platinum surfaces. Specifically, we would like to focus our attention on the potential region between +0.1 and -0.2 V where the current-potential response observed is ascribed to the adsorption of hydrogen to two energetically distinct sites: The peaks at 0.0 V and -0.15 V correspond to so-called strongly and weakly bound hydrogen, respectively. The voltammetry due to the platinum surface of the LSM (Figure 4.1b) shows only one pronounced (weakly bound) hydrogen adsorption peak characteristic of a clean well-ordered (i.e. atomically smooth over long-range) Pt(111) electrode (Figure 4.1c) which has been subjected to a few cycles in which a surface oxide layer is formed and removed (Figure 4.1d), resulting in a Pt(111) surface with nearly randomly distributed monoatomic steps[10].

We chose to study the underpotential deposition of copper on an iodine covered platinum surface. Iodine specifically adsorbs on platinum, chemically passivating the surface. This modification is extremely convenient from an experimental point of view, since we can first electrochemically clean the LSM's platinum surface and follow this immediately by adsorbing iodine, rendering the surface chemically impervious to contamination. In addition, XSW experiments on the electrosorption of iodide on a platinum/carbon LSM show that the I ad-layer seems to undergo similar potential dependent structural rearrangements on LSMs as Pt(111) single crystal electrodes[5]. The UPD of copper on such a surface has been shown to displace the iodine ad-layer and deposit directly onto the platinum surface[13]. Figure 4.2a shows the cyclic voltammetry for this system using a platinum/carbon LSM as the working electrode. This voltammetry is the result of following the steps described below:
(1) After cleaning the electrode surface (i.e. the LSM's surface) by a series of oxidation-reduction cycles at a sweep rate of 20 mV/sec, in pure supporting electrolyte (0.1M sulfuric acid) resulting in the voltammetry displayed in Figure 4.1b, and forming an iodine ad-layer by placing the clean electrode in contact with an iodide containing solution (1mM sodium iodide in 0.1M sulfuric acid) for approximately 15 min. at the rest (open circuit) potential, a small concentration of copper in introduced to the electrochemical cell (0.6mM cupric sulfate) and the rest potential is measured.

(2) A potential equivalent to this rest potential is applied to the electrode and a cycle is initiated by sweeping the applied potential negatively at 5 mV/sec. The cathodic current flow

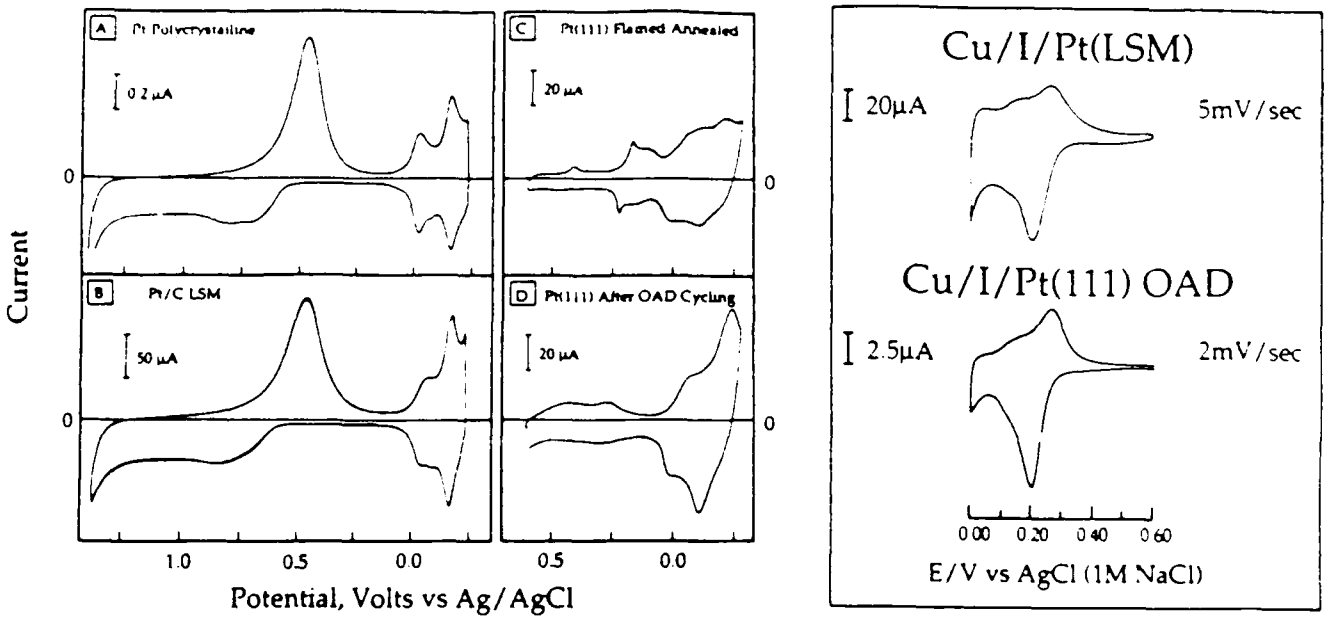

Figure 4.1 (right panel) Voltammetric profiles in 0.1 M H_2SO_4 of (A) polycrystalline Pt electrode (100 mV/s), (B) Pt/C LSM (100 mV/s), (C) clean, well-ordered Pt(111) electrode prepared by flame-annealing followed by quenching in PDW (50 mV/s), and (D) same electrode as in (C) after 10 oxygen adsorption-desorption cycles between +1.20 and -0.28 V at 50mV/s.

Figure 4.2 (left panel) (A) Cyclic voltammogram of the UPD of copper on an iodine covered platinum surface of a Pt/C LSM. (B) same as (A) but for a Pt(111) surface which has been reduced-oxidized through a series of cycles prior to iodine adsorption (see Figure 4.1).

observed between +0.4 and +0.1 V represents the underpotential deposition of a monolayer of copper onto the platinum surface.

(3) The cycle can be reversed at +0.05 V, just prior to the onset of bulk copper deposition, so that the applied potential is now swept positively at the same scan rate. The anodic current flow measured between +0.1 and +0.4 V represents stripping of the copper monolayer from the platinum surface into the bulk electrolyte solution.

A few important points should be made. First, the charge under the cathodic and anodic peaks is equivalent; all of the copper deposited on the surface is removed upon reversing the potential cycle. Second, the deposition process can be stopped by holding the applied potential at any value between +0.4 and +0.1 V, resulting in copper surface coverages ranging from 0 to 1 monolayer. Hence the ability to control precisely and reproducibly the surface coverage. Third, the cyclic voltammetry of copper UPD on a Pt(111) surface which has been oxidized-reduced a few times (Figure 4.2b) followed by the adsorption of iodine, is almost superimposable to that of the LSM, once again pointing out the structural correlation between these two types of surfaces.

The x-ray measurements were carried out while holding the applied potential at either +0.45, +0.25, +0.2, +0.15 or +0.1 V corresponding to copper surface coverages of 0, 1/4, 1/2, 3/4, and 1 monolayer respectively.

5. COVERAGE ISOTHERMS

Copper surface coverages were determined from both electrochemical and x-ray fluorescence measurements. Electrochemically, the coverage can be determined by integrating the charge under the cathodic and anodic current peaks in the cyclic voltammogram (Figure 4.2a). The charge can be transformed into a surface coverage assuming that:
(1) The following redox reaction is taking place during deposition:

$$Cu^{+2}_{sol} + 2\bar{e} \rightarrow Cu^{0}_{surf} \qquad (5)$$

implying that two electrons are transferred and that the deposited copper has no partial charge,
(2) The electrodeposited copper layer packs in a given surface structure, and
(3) The electrochemically active area of the electrode surface is known.
The surface coverages determined from electrochemical measurements, as shown in Figure 5.1a, assume that the copper overlayer forms an hcp structure with a Cu-Cu bond length of 2.556Å. The electrochemical area was determined by measuring the charge due to hydrogen adsorption in the cyclic voltammogram of Figure 4.1b.

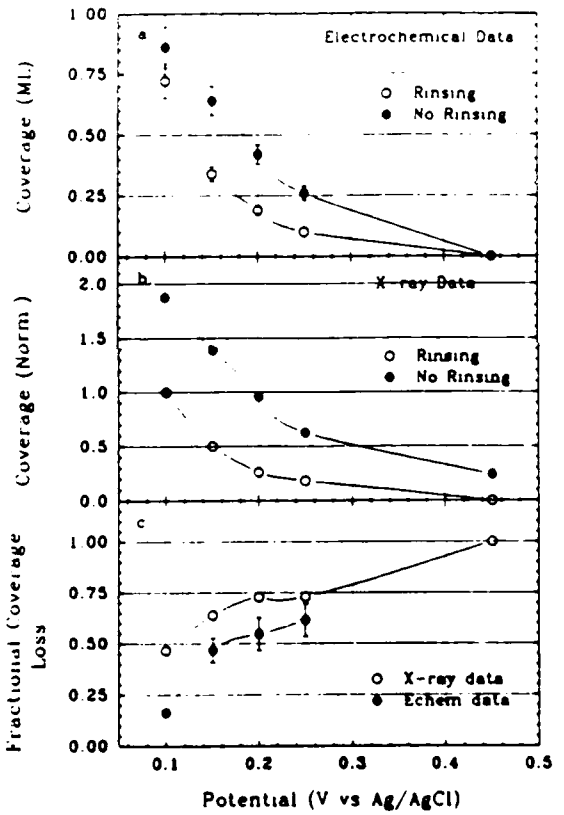

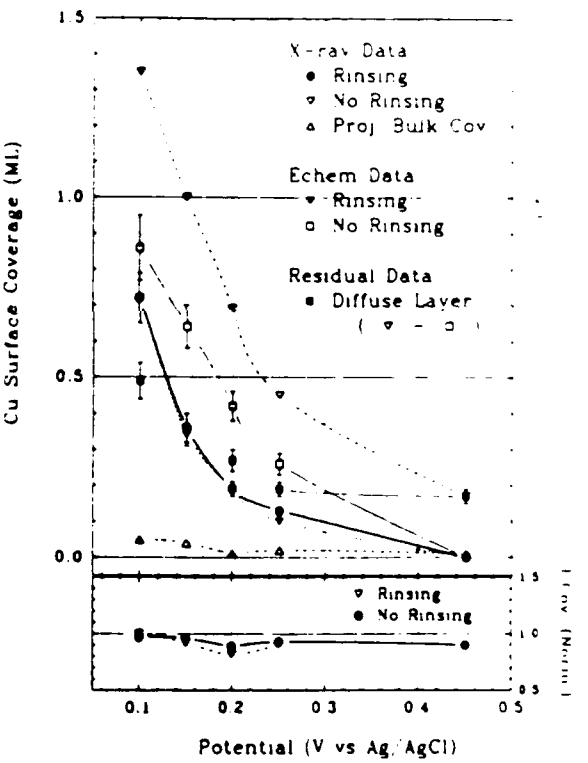

Figure 5.1 (right panel) (A) Copper coverage isotherms for rinsing and no rinsing experiments derived from electrochemical measurements. (B) same as (A) but for isotherms derived from x-ray fluorescence measurements. (C) the fractional coverage loss due to rinsing of the electrode surface with pure electrolyte, for both the electrochemical and x-ray data.

Figure 5.2 (left panel) X-ray and electrochemical derived isotherms plotted on an absolute coverage scale after the two data sets were normalized at one point, +0.1 V after rinsing.

Figure 5.1a, shows the surface coverage isotherms from two different sets of electrochemical experiments. In the first set of measurements, the deposited copper layer was stripped from the surface in the presence of bulk copper (no rinsing experiments). Under these conditions, the charge under the deposition and stripping peaks for various surface coverages is equal. In the second set of measurements, the deposited copper layer is stripped after rinsing the electrode three times with clean supporting electrolyte and with no bulk copper present in solution (rinsing experiments). In these experiments we observe a large discrepancy in the cathodic and anodic charge, the anodic peak always representing a smaller fraction of the charge measured under the cathodic wave. Figure 5.1a presents the surface coverage as determined from the anodic charge in cyclic voltammograms similar to that of Figure 4.2a, for the rinsing and no rinsing experiments discussed above. Comparing these isotherms, we observe a loss of deposited copper after rinsing, which is coverage dependent: at full monolayer coverage the loss is only 16% whereas for sub-monolayer coverages of 3/4, 1/2 and 1/4 we observe drastic losses of 47%, 55% and 62%, respectively. This behavior can be explained in part by referring to the Nerst equation describing the monolayer equilibrium potential E_{ML} as a function of the surface coverage Θ:

$$E_{ML} = E^0 + \frac{RT}{zF} \ln\left[\frac{f_{M^{z+}} c_{M^{z+}}}{\Theta f_{M^0}}\right] \tag{6}$$

where $f_{M^{z+}}$ and f_{M^0} are the activity coefficients of the metal ion in solution and the bulk deposit, E^0 is the standard potential for reaction (5), and $c_{M^{z+}}$ is the metal ion concentration in solution. From this equation we expect that for a given coverage Θ, E_{ML} will shift negatively as the bulk copper concentration is reduced. By rinsing the electrode with clean supporting electrolyte, we lower the copper solution concentration drastically resulting in a large negative shift in the monolayer equilibrium potential. Thus, at this point, the electrode is at an applied potential considerably more positive than the equilibrium potential E_{ML} for that given coverage, inducing a loss in the surface coverage. What we have not taken into account in this argument is the changes in the activity coefficients that the rinsing procedure will introduce. These changes are difficult to predict and as a result there is some uncertainty as to whether the Nerst equation (6) can account quantitatively for the changes we observe in the coverage.

The coverage isotherms determined from the off-Bragg data of the XSW fluorescence measurements are displayed on a normalized scale in Figure 5.1b. Once again we show two sets of data representing the outcome of equivalent rinsing and no rinsing experiments as the ones described above. Again, we observe a drastic loss of surface coverage after rinsing the electrode. However the fractional losses seen in these x-ray experiments are considerably larger than those measured electrochemically. In an attempt to quantify the x-ray derived isotherms they have been plotted on an absolute scale versus the electrochemical ones normalizing the two data sets at only one point: 0.1V, after rinsing (Figure 5.2). We note that the coverage isotherms for both the x-ray and electrochemical rinsing experiments are in good agreement, but when we compare the results of experiments where the electrode had not been rinsed, the x-ray measurements indicate the presence of a considerable amount of electrochemically inactive copper, above and beyond the bulk copper present in solution. In addition, XSW measurements corresponding to this coverage place this excess copper at the solid/solution interface. Furthermore, even at applied potentials of +0.45 V, where no deposition has yet occurred, we observe an amount of copper equivalent to approximately 2/10 of a monolayer. Finally, we note that the iodine coverage as determined from x-ray fluorescence, is constant throughout the experiment (Figure 5.2).

From these measurements of coverage we can conclude that:
(1) There is a drastic loss of surface coverage upon rinsing the electrode with clean supporting electrolyte, this loss is explicable in terms of the Nerst equation implying that the underpotential deposition of copper on an iodine pre-treated platinum surface is an reversible process.
(2) A comparison of isotherms from x-ray and electrochemical measurements after rinsing shows excellent agreement. However when we compare the results from no rinsing experiments, the x-ray derived isotherm reveals the presence of a considerable additional amount of electrochemically inactive copper.
(3) This excess copper is located at the solid/liquid interface, and is present even at potentials where no deposition of copper has taken place. In addition, the amount of excess copper is potential dependent, and seems to be only weakly adsorbed since it can be rinsed away.

6. REFLECTIVITY MEASUREMENTS

Reflectivity measurements are quite valuable in characterizing important structural features of the substrate. Specifically, from a reflectivity measurement one can determine the thickness of the thin solution layer trapped between the LSM and the polypropylene film encapsulating the electrochemical cell, and the LSM's interfacial and surface roughness. Figure 6.1 shows the angular dependence of the measured absolute Bragg reflectivity for a platinum/carbon LSM under a solution layer 0.98 μm thick. The net effect of interfacial roughness is to enhance the transmission of x-rays through the LSM, resulting in a decrease of the peak reflectivity and a sharpening of the reflection profile, since the LSM's reflection width $\Delta\theta/\theta$ is inversely proportional to the effective number of layers participating in Bragg diffraction. The interfacial roughness was modeled by a Debye-Waller term of the form

$$\exp\left\{\frac{-4\pi\sigma\sin\theta}{\lambda}\right\}^2 \tag{7}$$

where σ is the rms interfacial roughness. In this approach a Gaussian distribution describes the roughness as a function of depth about the average of the roughness profile.

The solution layer thickness can be easily calculated according to

$$R_{Measured} = R_{Emersed} T_{Polypro} T_{Solution} \tag{8}$$

where $R_{Emersed}$ refers to the measured LSM reflectivity *ex situ*, $T_{Polypro}$ and $T_{Solution}$ are transmission coefficients expressed as

$$T = \exp\left\{-\frac{2t}{\sin\theta}\mu\right\} \tag{9}$$

Since the linear absorption coefficient and the thickness of the polypropylene layer are well know, $T_{Solution}$ and the solution layer thickness can be accurately determined.

The low reflectivity observed in the specular reflectivity profiles (Figure 6.2) below 2 mrad is due to the projection of the 0.040mm incident beam height onto the sample's surface oversubtending the 20 mm length of the sample. With no solution layer present, the remaining portion of the reflectivity profile prior to the LSM's critical angle at 6.55 mrad, is smooth with a maximum reflectivity of only 45% due to the attenuation from the polypropylene film. When the solution layer is present, the reflectivity profile shows a peak around 3.0 mrad corresponding to specular reflection from the solution layer. Beyond this angle, the reflectivity drops to 20% because of the added attenuation of the solution layer. Above the LSM's critical angle, the reflectivity drops precipitously and is extremely sensitive to surface roughness. From the Bragg reflectivity measurements we determined the interfacial roughness to be

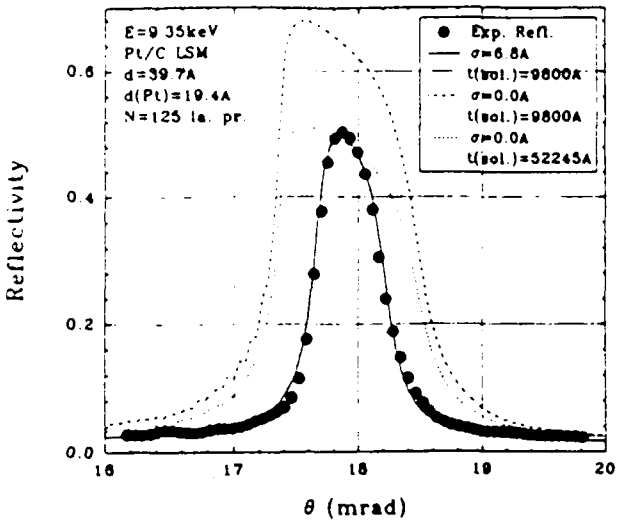

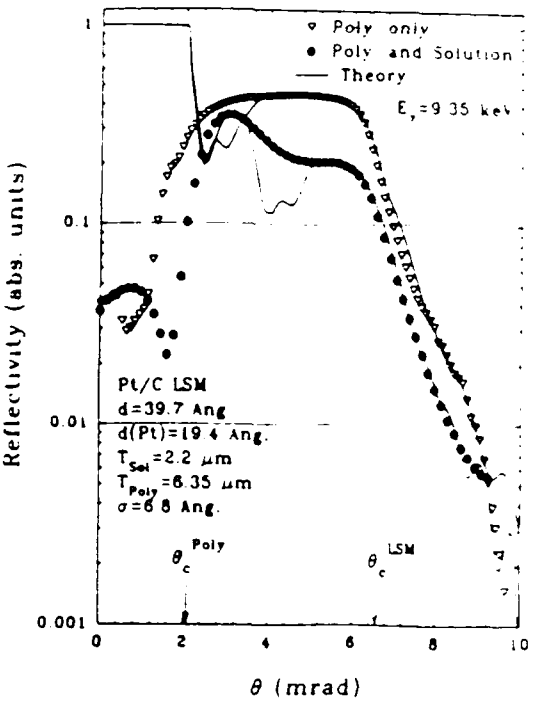

Figure 6.1 (right panel) Angular dependence of the measured absolute Bragg reflectivity (filled circles) for a Pt/C LSM under a solution layer 9800 Å thick, encapsulated by a 6.35μm polypropylene film. The dashed line represents the theoretical prediction for the reflectivity when the interfacial roughness of the substrate is neglected. The dot line represents a calculation attempting to fit the experimental data by increasing the solution layer thickness, while continuing to neglect the interfacial roughness. The solid line represents the best fit to the data.

Figure 6.2 (left panel) Total external reflection profiles a Pt/C LSM covered by a polypropylene layer only (open triangles), and the same Pt/C LSM under a solution layer as well as the polypropylene film (filled circles). The solid lines represent the best theoretical fits to the data.

6.8±0.5 Å. Assuming this roughness value for the surface produced a good fit to the specular reflectivity data as well.

7. X-RAY STANDING WAVE MEASUREMENTS

In this section we will discuss initial results from the analysis of the standing wave fluorescence data corresponding to the rinsing experiments discussed above. Specifically, we measured the standing wave profiles for both specular reflection and Bragg diffraction after depositing at potentials of +0.25, +0.20, +0.15 and +0.1V and rinsing the electrode with clean supporting electrolyte (no copper present in solution) while maintaining potential control over the system at all times.

The background subtracted Cu K_α XSW fluorescence yield was extracted from each fluorescence spectrum (in energy dispersed form) by fitting to a Gaussian on a quadratic background. The extracted yields from each angular interval in a given scan were then

normalized to the live time, taking into account dead time effects, and combined to give the Cu K fluorescence vs θ profiles presented in Figures 7.1 and 7.2. This experimental data was χ^2 fitted to the theoretical yields calculated from the integral (4) using a Poisson distribution for N(z). The free parameters in these fits were: the distribution's peak position with respect to the substrate's surface, the distribution's FWHM, and a normalizing constant directly proportional to the distribution's area. In addition, XSW data from the specular and Bragg reflection regions were fitted simultaneously.

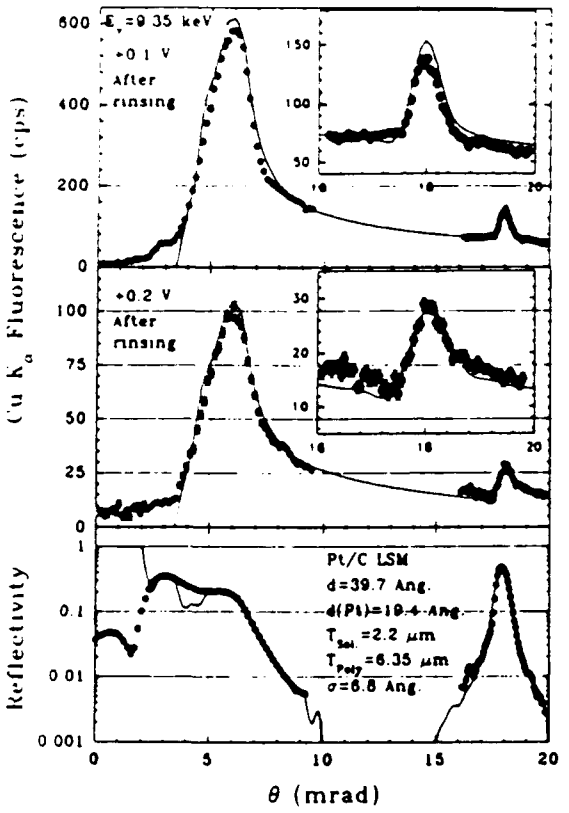

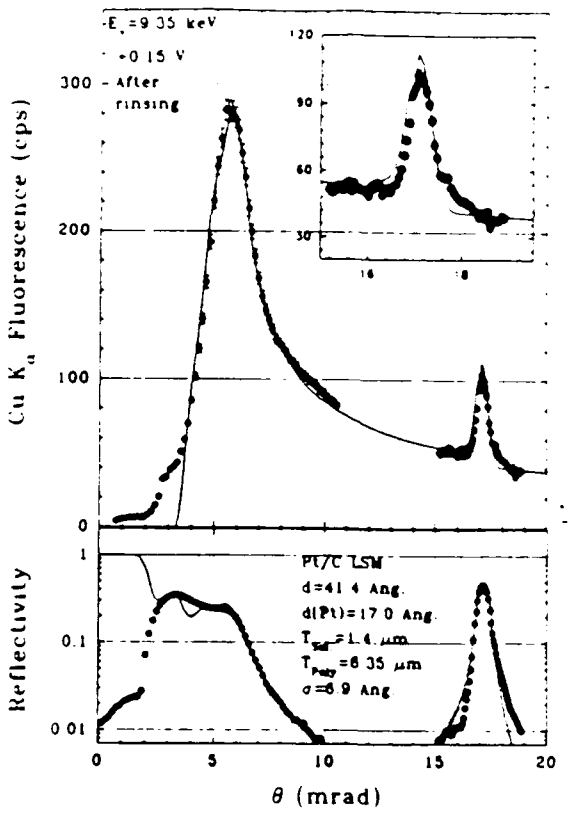

Figure 7.1 (right panel) The XSW fluorescence profiles for both the specular reflectivity and Bragg diffraction domains for +0.1V and +0.2V after rinsing the electrode surface with clean electrolyte. A magnified view of the Bragg data is show in the insets. Also shown at the bottom, is the complete reflectivity profile. Fits of the data were performed over the entire angular range simultaneously, and are plotted as solid lines.

Figure 7.2 (left panel) Same as Figure 7.1 but at +0.15 V after rinsing, using a Pt/C LSM with a slightly different d-spacing.

The theoretical yields were calculated using a computational scheme based on a stratified interface formalism[12] which allows for the inclusion of the solution and polypropylene layers along with the LSM in a single model, having the advantage of being exact by taking both refraction and absorption properly into account. In addition, we took into account two geometrical corrections. The first accounted for the changes in the sample volume illuminated by the finite height of the beam as θ is increased. The second corrected the increase in fluorescence as θ was increased due to the finite solid angle subtended by the solid-state detector. The best theoretical fits are shown as solid lines on Figures 7.1 and 7.2.

During specular reflection, the incident x-ray traveling wave is forbidden to penetrate trough a mirror surface, and as a result the Cu K_α fluorescence count rate for the data shown in Figures 7.1 nd 7.2 is very low at angles smaller than the solution layer critical angle of 3.4 mrad. The angular behavior of the standing wave generated during specular reflection can be described as follows. At θ=0 a node of the standing wave is at the surface and the first antinode is at infinity. As the angle of incidence is increased, the first antinode moves inward, in a direction normal to the surface, until at the critical angle, θ_c of the LSM it coincides with the surface. The trailing antinodes follow behind with a periodic spacing given by 1/Q (see equation 3). At the LSM's critical angle the standing wave period D_c is 100 Å for the LSM used in the experiments at +0.1, +0.2 and +0.25 V (Figure 7.1), and 120 Å for the LSM used at +0.15 V (Figure 7.2). Keeping the above discussion in mind, we note that in all cases studied, the first XSW antinode passes over the center of mass of the copper density as we reach the critical angle of the LSM. This means that a narrow distribution of copper exits at the LSM surface for all of the potentials investigated. However, since the critical XSW periodicity D_c is in all likelihood much larger then the extent of the copper distribution in the cases illustrated, the resolution to which we can determine the distribution's position and width is fairly poor.

To improve the resolution we can make use of the XSW measurements in the Bragg regime, where the periodicity of the standing wave is essentially equivalent to the LSM's d-spacing. Referring to the insets of Figures 7.1 and 7.2, we observe rather different XSW profiles as a function of applied potential. The expected yield for a random distribution is proportional to:

$$Y_{Off\text{-}Bragg}[1+R(\theta)] \qquad (10)$$

but in all cases shown here, the fluorescence peak amplitude to background ratio is well beyond this random limit, indicating that the copper distribution is fairly narrow on the length scale of the standing wave period. The changes in the shape of each standing wave profile are representative of changes in the position of this overlayer with potential, although these changes do not appear to be very large since the peak angular position, taken with respect to the Bragg angle, in each standing wave signal is nearly the same. It is also important to note that in this regime, positional information is referenced to the diffraction planes of the LSM, not the surface. This could be a source of uncertainty in locating an overlayer's position with respect to the substrate's surface as that overlayer may not be necessarily positioned on the surface. In addition, it can lead to ambiguities when positional changes observed in a given experiment span a range larger than the characteristic modulo-d periodicity of XSW generated by Bragg diffraction. Fitting XSW data generated in the specular reflection and the Bragg diffraction regimes simultaneously, allows us to probe the same distribution of species on two rather different length scales and two different z-scale origins, leading to an unambiguous result.

Figure 7.3 summarizes the standing wave results in terms of the distribution profiles at each potential studied. In the main panel all distribution profiles are normalized to the same peak intensity, while in the inset we show each distribution in terms of their relative areas. Also shown is the surface density profile on a normalized scale as determined from the fits to the reflectivity data. Note that the origin of the z scale is defined to be where bulk platinum begins. The potential/coverage dependent changes in the peak position and FWHM of these distributions can be better visualized in figures 7.4 and 7.5. The peak position increases with increasing coverage as the applied potential is made more negative. When plotted against the applied potential, the peak position can be fitted empirically by an equation of the form:

$$a-\exp(b\varphi) \qquad (11)$$

where φ is the applied potential, a=8.46±0.20 Å and b=7.06±0.22 1/V. The FWHM increases linearly with potential with a slope of -38.6±0.3 Å/V and a y-intercept of 16.5 Å. It is

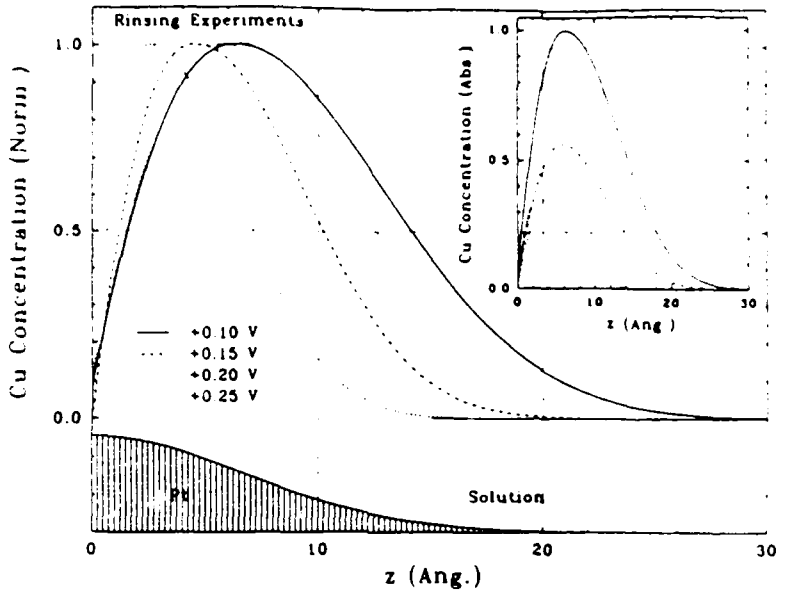

Figure 7.3 Copper concentration profiles after rinsing vs. distance z normal to the LSM's surface, derived from the analysis of the standing wave data. In the main panel all distributions are normalized so that the peak concentration is one. The inset shows the same concentration profiles in terms of their relative areas.

interesting to note that at a FWHM of zero (x-axis intercept), the applied potential is 0.43 V which corresponds to the onset of copper UPD (see figure 4.2a). In addition to the distribution's parameters we also plot (Figure 7.6b,c) the center of mass (i.e. the z-position where we reach 50% of the total amount of copper) of each distribution as a function of both applied potential and coverage. This particular quantity is revealing, since it is dependent on both the peak position and the FWHM in a given distribution. In order to explain the changes we observe in this parameter we need to consider the surface morphology in terms of the Gaussian model we have chosen to use to fit the reflectivity data. This model is illustrated in Figure 7.6a, where we plot the fractional concentration of surface sites as a function of position along the z-scale (the Gaussian's area is normalized to one). Note that the origin in the z axis corresponds to the one illustrated in Figure 7.3. In addition, we have sectioned this concentration profile (Figure 7.6a) into bins with a width approximately equal to the the closest packing distance for platinum (2.26 Å) in order to introduce a finite size effect. If open surface sites were occupied in a random mode, one would expect a homogeneous copper distribution whose center of mass was always at the same z position, namely the center of the Gaussian representing the surface sites concentration profile (i.e. the position with the largest density of open sites). At the opposite extreme, we have a model in which open surface sites are occupied sequentially with the deepest (closest to z=0 Å) ones first. In this case, the center of mass position would vary with the copper surface coverage. Both of these models are plotted with the experimental data in Figures 7.6b,c. Although quantitatively the data does not fit either model well, it is clear that the observed trends are in better agreement with the picture where sequential filling of available surface sites with the deepest ones being occupied first, does occur. This finding implies that the more favorable surface sites for deposition are the ones closest to the platinum bulk lattice, either because the substrate-deposit interactions are maximized at these sites, or because the interaction with the electric fields present at the interface is greatest at these locations. In addition, deposited copper atoms either diffuse to these positions or the deposition process itself is "catalyzed" by these particular sites.

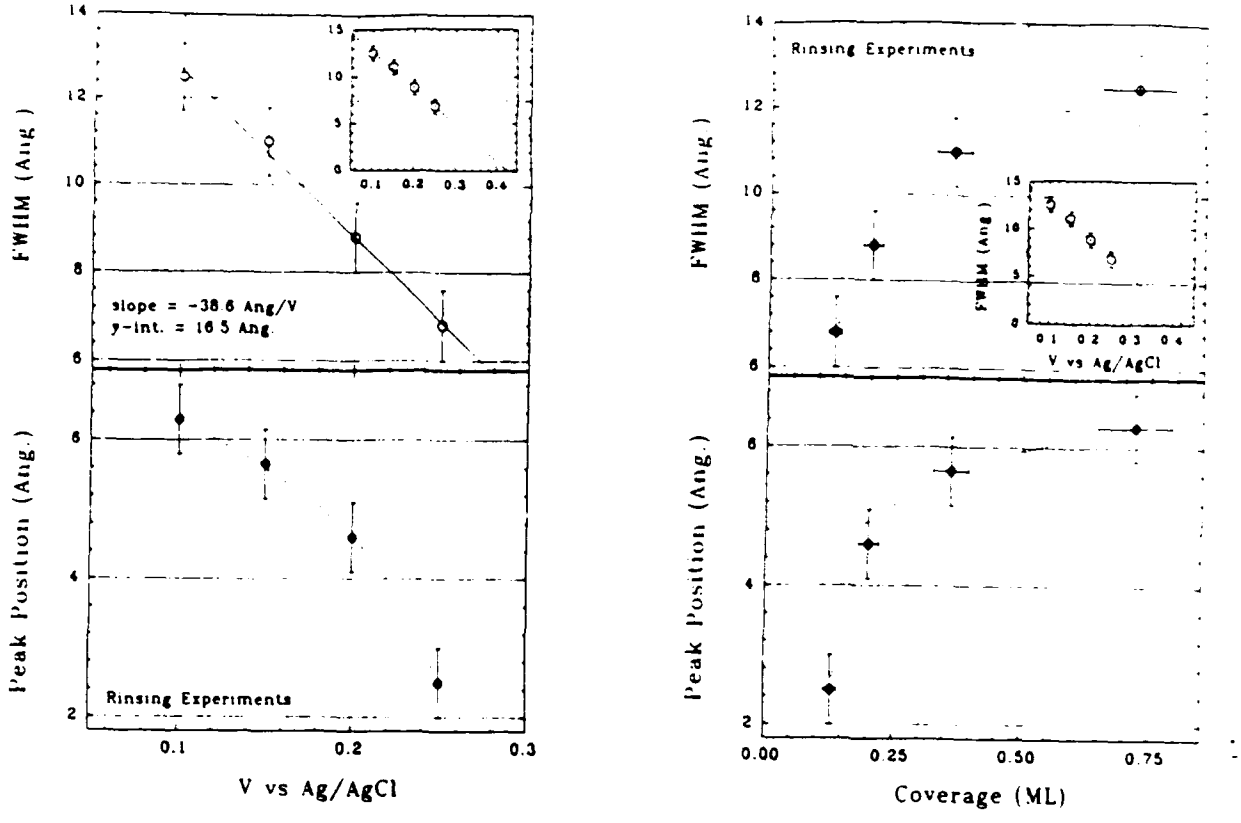

Figure 7.4 (right panel) Peak position and FWHM from the copper concentration profiles of Figure 7.3 as a function of the applied potential.

Figure 7.5 (left panel) Same as Figure 7.4 but versus the copper coverage (see Figure 5.2).

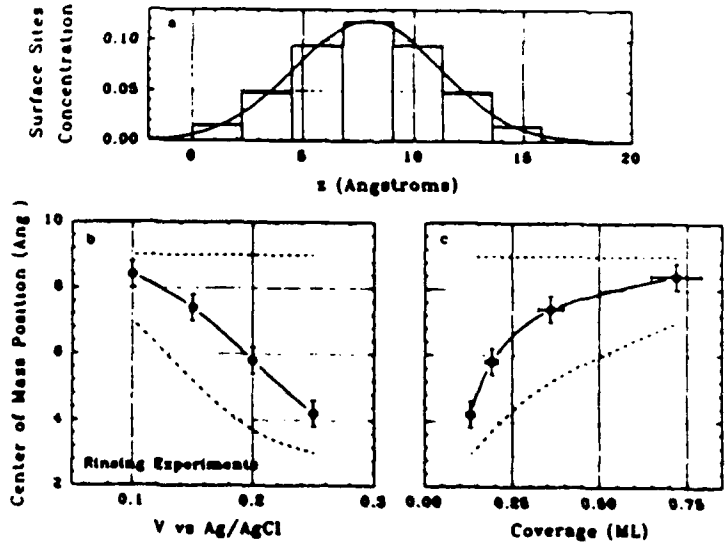

Figure 7.6 (A) Shows the fractional concentration of surface sites as a function of the distance z, based on the model used to the determine the surface roughness at the platinum/solution interface, and where the z-scale is the same one defined in Figure 7.3. The area of the

Figure 7.6 (cont.) Gaussian is normalized to one. (B) and (C) show the variation of the center of mass in the copper distributions of Figure 7.3, as a function of applied potential and coverage. The top horizontal dashed line in each panel represents the expected variation in the center of mass for a model in which filling of the bins in (A) is random, whereas the dashed lines at the bottom of (B) and (C) represent the variation expected for a model where the bins in (A) are filled sequentially starting with the deepest one (closest to z=0 Å) first.

Furthermore, we should consider whether the nature of the deposition process is coverage dependent, since lateral interactions among deposited atoms might become more important as the coverage is increased, and what structural role iodine might play. It is also unclear what structural effect rinsing the electrode surface with pure electrolyte has on the UPD layer. It is likely that some structural rearrangement will be triggered by this rinsing procedure. A comparison of the data shown here with results from XSW experiments were the electrode is not rinsed (under investigation at this moment), should provide the answers to these questions.

8. CONCLUSIONS

We were able to study *in situ*, the underpotential deposition of copper on an iodine covered platinum/carbon layered synthetic microstructure, using XSWs generated by specular (total external) reflection and Bragg diffraction. The equilibrium structure of the UPD layer after rinsing of the electrode surface with pure electrolyte is one where the deposited copper density is highest for those surface sites closest to the bulk platinum lattice. In addition, we were able to follow potential dependent changes in the copper surface coverage as determined by independent electrochemical and x-ray measurements. We observe a loss of surface coverage upon rinsing, and a good correlation between the electrochemical and x-ray data. However, x-ray derived isotherms resulting from no rinsing experiments reveal the presence of a large excess of electrochemically inactive copper at the solid/solution interface, when compared to the corresponding electrochemically derived isotherms.

9. ACKNOWLEDGMENTS.

This work was supported by the Materials Chemistry Initiative of the National Science Foundation and by the Office of Naval Research. H.D.A is the recipient of a Presidential Young Investigator Award (1984-1989) and a Sloan Foundation Fellow (1987-1991). The authors are grateful for the contributions made by Donna Taylor and Howell Yee.

10. REFERENCES

1. a. Kolb,D.M., in H. Gerisher and C. Tobias, eds., Advances in Electrochemistry and Electrochemical Enginneering, Vol. 11, J. Wiley and Sons, New York, *1978.*
   b. Adzic, R. *Isr. J. Chem.* 18,166,*1979.*
   c. Adzic, R., in H. Gerisher and C. Tobias, eds., Advances in Electrochemistry and Electrochemical Enginneering, Vol. 13, J. Wiley and Sons, New York, *1985.*
2. a. Schultze, J.W.; Dickertmann, D. *Symp. Faraday Soc.* 12,36,*1977.*
   b. Salvarezza, R.C.; Vasquez Moll, D.V.; Giordana, M.C.; Arvia, A.J. *J. Electroanal. Chem.* 213,301,*1986.*
   c. Parajon Costa, B.; Canullo, J; Vasquez Moll, D.V.; Salvarezza, R.C.; Giordano, M.C.; Arvia, A.J. *J.Electroanal. Chem.* 244,261,*1988.*

3. a. Schultze, J.W.; Dickertmann, D. *Surf. Sci.* **54**,489,*1976.*
   b. Bewick, A.; Thomas, B. J. *Electroanal. Chem.* **70**,239,*1976.*
4. Beckmann, H.O.; Gerisher, H.; Kolb, D.M.; Lehnpfuhl, G. *Symp. Faraday Soc.* **12**,51,*1977.*
5. a. Stickney, J.L.; Rosasco, S.D.; Song, D.; Soriaga, M.P.; Hubbard, A.T. *Surf. Sci.* **130**,326,*1983.*
   b. Hubbard, A.T.; Stickney, J.L.; Rosasco, S.D.; Soriaga, M.P.; Song, D. *J. Electroanal. Chem.* **150**,165,*1983.*
   c. Stickney, J.L.; Rosasco, S.D.; Hubbard, A.T. *J. Electrochem. Soc.* **131**,260,*1984.*
6. a. Magnussen, O.M.; Hotlos, J; Nichols, R.J.; Kold, D.M.; Behm, R.J. *Phys Rev Lett.* **64**,2929,*1990.*
   b. Manne, S.; Hansma, P.K.; Massie, J.; Elings, V.B.; Gewirth, A.A. *Science* **251**,183,*1991.*
7. a. Abruña, H.D.; White, J.H.; Albarelli, M.J.; Bommarito, G.M.; Bedzyk, M.J.; McMillan, M.J. *J. Phys. Chem.* **92**,7045,*1988.*
   b. Tourillon, G.; Guay, D.; Tadjeddine, A. *J. Electroanal. Chem.* **289**,263,*1990.*
   c. Tadjeddine, A. J.; Guay, D.; Ladouceur, M.; Tourillon, G. *Phys. Rev. Lett.* **66**,2235,*1991.*
8. a. Samant, M.G.; Toney, M.F.; Borges, G.L.; Blum, L.; Melroy, O.R. *J. Phys. Chem.* **92**,220,*1988.*
   b. Toney, M.F.; Gordon, J.G.; Samant, M.G.; Borges, G.L.; Wiesler, D.G.; Yee, D.; Sorensen, L.B. *Langmuir* **7**,796,*1991.*
9. a. Bedzyk, M.J.; Bommarito, G.M.; Caffrey, M.; Penner, T. *Science* **52**,248,*1990.*
   b. Bommarito, G.M.; White, J.H.; Abruña, H.D. *J. Phys. Chem.* **94**,8280,*1990.*
10. Aberdam, D.; Durand, R.; Faure, R.; El-Omar, F. *Surf. Sci.* **171**,303,1986.
11. a. Lu, F.; Salaita, G.N.; Baltruschat, H.; Hubbard, A.T.; *J. Electroanal. Chem.* **222**,305,*1987.*
   b. White, J.H.; Abruna, H.D. *J. Phys. Chem.* **92**,7131,*1988.*
12. a. Parratt, L.G. *Phys. Rev.* **95**,359,*1954.*
   b. Bommarito, G.M.; M.S. Thesis, Cornell University, *1987.*